

Bidirectional Captioning for Clinically Accurate and Interpretable Models

Keegan Quigley¹, Miriam Cha¹, Josh Barua^{1,2}, Geeticka Chauhan³,
Seth Berkowitz^{4,5}, Steven Horng^{4,5}, Polina Golland³

¹MIT Lincoln Laboratory ²UC Berkeley ³MIT CSAIL

⁴Beth Israel Deaconess Medical Center ⁵Harvard Medical School

{keegan.quigley,miriam.cha}@ll.mit.edu, joshbarua@berkeley.edu, geeticka@mit.edu,
{sberkowi,shorng}@bidmc.harvard.edu, polina@csail.mit.edu

Abstract

Vision-language pretraining has been shown to produce high-quality visual encoders which transfer efficiently to downstream computer vision tasks. While generative language models have gained widespread attention, image captioning has thus far been mostly overlooked as a form of cross-modal pretraining in favor of contrastive learning, especially in medical image analysis. In this paper, we experiment with bidirectional captioning of radiology reports as a form of pretraining and compare the quality and utility of learned embeddings with those from contrastive pretraining methods. We optimize a CNN encoder, transformer decoder architecture named RadTex for the radiology domain. Results show that not only does captioning pretraining yield visual encoders that are competitive with contrastive pretraining (CheXpert competition multi-label AUC of 89.4%), but also that our transformer decoder is capable of generating clinically relevant reports (captioning macro-F1 score of 0.349 using CheXpert labeler) and responding to prompts with targeted, interactive outputs.

Introduction

Automated medical image analysis has the potential to revolutionize healthcare diagnostics, but its efficacy is often constrained by the limited availability of annotated data. Acquiring high-quality annotations is time-consuming and requires expert knowledge, making fully supervised modeling approaches impractical.

The vast repository of radiology reports—unstructured textual descriptions paired with radiographs—offers a valuable resource. By leveraging these paired reports, it is feasible to improve the quality of visual representations and mitigate the challenges posed by limited labeled data. Recently, contrastive learning has gained attention with impressive results shown in various domains. Notably, CONVIRT (Zhang et al. 2022) first demonstrated dual-encoder contrastive learning with radiology reports to improve image representations, and CheXzero (Tiu et al. 2022) highlighted the impressive zero-shot capabilities of a dual-encoder architecture. However, a limitation of methods based on contrastive learning is their inability to provide interpretable outputs akin to comprehensive radiology reports. By probing the visual embedding with textual embeddings, an indirect interpretation can be achieved but this requires careful

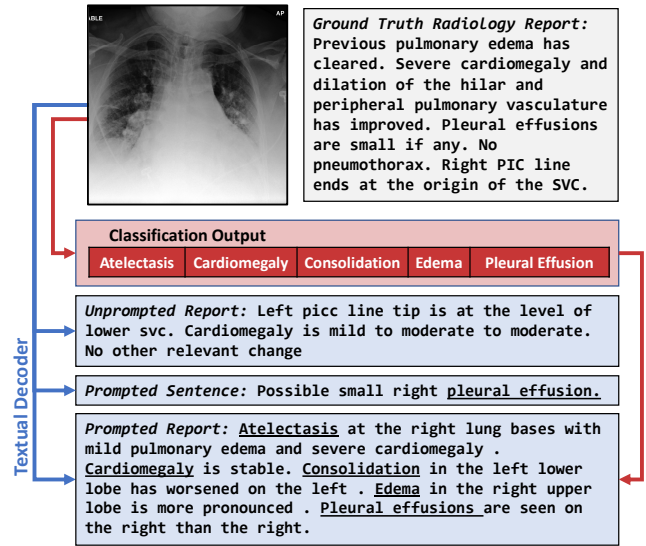


Figure 1: Overview of RadTex outputs for interpretability

formulation of textual inputs, and is not fully studied beyond classification tasks. Thus, while contrastive learning based methods improve visual representations, further steps are necessary to ensure these models deliver clinically meaningful and understandable results.

In this work, our objective is twofold: improve medical image representations and simultaneously generate interpretable radiology reports. We present RadTex, a pre-training approach using bidirectional captioning to learn medical image representations. Figure 1 provides a visual explanation of the RadTex capabilities. Given an image, RadTex is able to utilize visual embeddings to output classification labels and a detailed radiology report (i.e. unprompted report). In an automated diagnostics advancement, RadTex can also process user-specified textual prompts. For example, given an image and a prompt pleural effusion, RadTex generates Possible small right pleural effusion providing image-aligned explanations. Furthermore, RadTex can ingest discrete classification labels, translating them into detailed diagnostic narratives elucidating each classification output. To

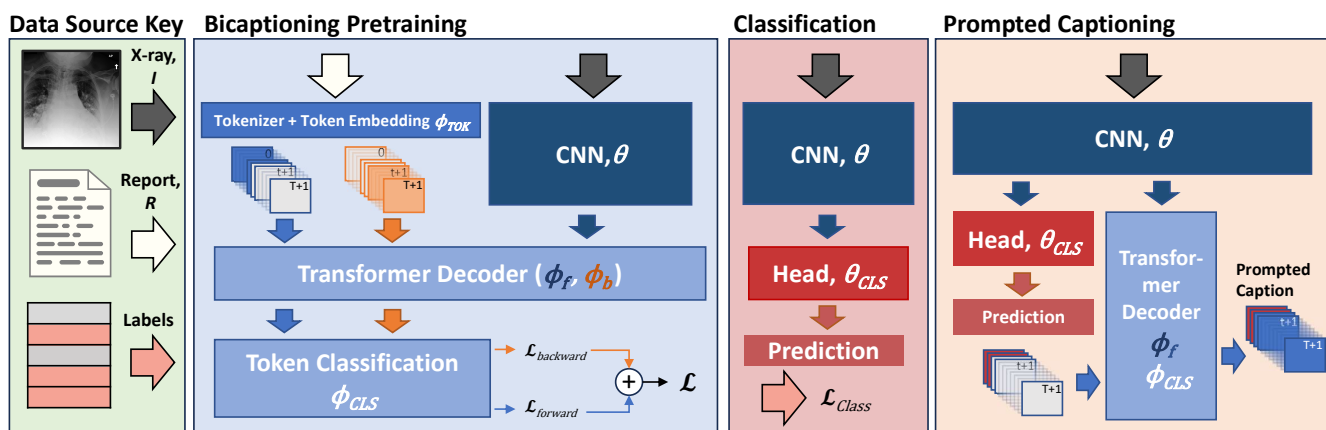


Figure 2: RadTex architecture overview, showing available training data, bidirectional captioning for pretraining, downstream classification training, and prompted captioning. In prompted captioning, the outputs from the classification module are used to construct the starting sequence for forward captioning. Note that the arrows in the *Data Source Key* pane denote which input is applied during training and inference in the other panes.

the best of our knowledge, this is the first framework to prompt a transformer decoder with textual inputs to output interpretable pathological findings.

While providing a flexible prompting mechanism that outputs interpretation of diagnostics, RadTex achieves competitive performance compared to state-of-the-art contrastive learning methods. On the CheXpert competition dataset, we achieve 89.4% AUC with frozen linear classification, which is a 0.4% improvement over the best contrastive learning method. The gain in performance is accompanied by increased interpretability. Our main contributions are summarized below:

- We present optimal architecture and hyperparameters for RadTex, extending the contributions of VirTex (Desai and Johnson 2021) for data-efficient pretraining to the radiology domain.
- We show that the bicapting pretraining task is competitive with contrastive image-text pretraining for learning strong visual representations that transfer efficiently to downstream medical image classification tasks.
- We demonstrate RadTex’s capability to generate clinically accurate radiology reports using flexible user-driven prompts, indicating a promising avenue for enhanced radiologist-AI interaction.

Related Work

Our work is most relevant to vision-language pretraining in the medical domain and automated radiology report generation.

Vision-Language Pretraining While great strides have been made in supervised deep learning using convolutional neural networks and transformers (He et al. 2015; Vaswani et al. 2017; Dosovitskiy et al. 2021), limited labeled examples and time-consuming annotation in the medical domain limit progress of such approaches. Two approaches have been effective at countering this labeled data barrier:

the release of large-scale weakly annotated datasets (Irvin et al. 2019; Johnson et al. 2019b) and the development of self-supervised vision-language modeling.

ConVIRT (Zhang et al. 2022) first proposed adapting contrastive learning (Chen et al. 2020) to vision-language tasks for learning visual representations. Their work inspired Radford et al. (2021), whose CLIP model quickly became state-of-the-art for natural image-text representation learning. CLIP’s dual-encoder architecture has been adapted back to radiology as CheXzero (Tiu et al. 2022), and improved with more careful selection of image-text pairs (Wang et al. 2022) and in-domain pretraining (Mishra et al. 2023).

Additionally, self-supervised learning approaches in the general domain have utilized encoder-decoder architectures for image-text pretraining (Lu et al. 2019; Li et al. 2020; Zhou et al. 2020). Recently, Yu et al. (2022b) demonstrated the impressive potential of such encoder-decoder architectures as foundation models that can be transferred to downstream tasks by using contrastive and captioning losses. (Zhang et al. 2022) experimented with a Meshed Memory transformer for learning visual representations, but found performance worse than contrastive learning. Our architecture, inspired by VirTex (Desai and Johnson 2021), employs an encoder-decoder architecture, learning visual representations with a bidirectional image captioning task. This approach not only produces interpretable radiology reports but also offers competitive performance compared to contrastive learning techniques in downstream vision tasks.

Radiology Report Generation Many authors have proposed methods for radiology report generation from chest X-rays, which have the potential to improve clinical interpretability of deep learning methods by describing clinical observations in plain text. The image-captioning task has been studied extensively in the natural image domain (Vinyals et al. 2015; Stefanini et al. 2023), but captioning in the radiology domain has distinct challenges which require unique approaches. To address challenges of linguis-

tic and semantic consistency of generated reports, which are typically longer than natural image captions, many authors have proposed using hybrid retrieval-generation models or templates (Li et al. 2018; Pino et al. 2021). Endo et al. (2021) proposed a report generation system that uses vision-language pretraining to improve retrieval.

Others have explored neural text generation for radiology, which has the potential to generate observations and relations purely based on the image. (Jing, Xie, and Xing 2018) and (Wang et al. 2018) use LSTM-based generation, while (Miura et al. 2021) and (Chen et al. 2022) utilize transformers (Vaswani et al. 2017) to generate relevant clinical information. Many of these encoder-decoder architectures utilize a semantic feature extractor to focus generation on clinically relevant observations, and we build on their approaches with *Prompted Captioning*.

Method

We introduce RadTex, which employs bidirectional captioning (*bicaptioning*) as a pretraining approach for interpretable medical image analysis. The overall framework is presented in Figure 2. We adopt the bicaptioning framework by Desai and Johnson (2021) to implement the RadTex model.

Pretraining

Pretraining consists of jointly training an image encoder and a text decoder via bidirectional image captioning. Training begins with a ResNet50 (He et al. 2015) as our visual encoder, extracting visual features from an X-ray image I . We take the output of the last convolutional layer as spatial image features, and use a linear projection to create a sequence of image features for “translation,” which we call x_{vis} . A paired radiology report R is processed by tokenizer ϕ_{TOK} , and resultant tokens $w = \{w_0, \dots, w_{T+1}\}$ make up the input sequence of length $T + 2$, including the special [SOS] and [SEP] tokens at either end. Each token $w_i \in D$, the vocabulary of the tokenizer. Tokens w are encoded by a learned word and positional embedding into a textual sequence x_{text} .

Textual decoding during pretraining is carried out by a transformer decoder (Vaswani et al. 2017) with self-attention and multihead attention modules. The t -th token w_t in the report is predicted twice by the transformer decoder during pretraining: once forward and once backward. In each layer of the forward transformer decoder, masked multiheaded self-attention is applied to the input token embeddings x_{text} (token embeddings after t are masked), followed by multiheaded attention applied to both transformed token embeddings and the visual embedding sequence x_{vis} . Between these attention modules, element-wise sum, layer normalization, and dropout are applied and residual connections are made around attention layers. This architecture is duplicated for the backward captioning transformer, and textual sequence is reversed before input.

At the output of the last transformer layer, a single linear layer (weights shared between forward and backward decoders) is applied to predict the element of the vocabulary. We compute cross entropy loss to measure the difference

between predicted token and the ground truth, minimizing negative log-likelihood as follows:

$$L = - \sum_{t=1}^{T+1} \log p(w_t | I, w_{i < t}; \theta, \phi_f) - \sum_{t=0}^T \log p(w_t | I, w_{i > t}; \theta, \phi_b) \quad (1)$$

Here, $w_{i < t}$ and $w_{i > t}$ represent the tokens appearing before and after the t -th token respectively. The parameter θ corresponds to the parameters of the image encoder and ϕ_f and ϕ_b represent the parameters for the forward and backward decoders. In this way, prediction of w_t is conditioned on $\{w_{i < t}, x_{vis}\}$ for forward captioning and $\{w_{i > t}, x_{vis}\}$ for backward captioning.

Explainable Captioning

Given the pretrained ability to predict the probability of a token w_t with either $\{w_{i < t}, x_{vis}; \phi_f\}$ or $\{w_{i > t}, x_{vis}; \phi_b\}$, we can utilize our learned model from pretraining for autoregressive captioning. Autoregressive captioning uses an iterative approach to build up a caption from an initial sequence, appending a token at each step. During each step, token probabilities are computed using the frozen visual encoder and textual decoder, conditional on the input image I and the pre-existing tokens in the sequence. An algorithm (denoted η) such as beam search or nucleus sampling (Holtzman et al. 2020) can then be used to sample a token from the computed probabilities. We formalize our autoregressive captioning in Algorithm 1.

Algorithm 1 Autoregressive Prompted Captioning

Input: Prompt P ; Sampling Strategy η ; Image I
Output: Caption tokens w

- 1: $x_{vis} \leftarrow \theta(I)$ ▷ Visual Embedding
- 2: $w \leftarrow [\phi_{TOK}([SOS]), \phi_{TOK}(P)]$ ▷ Tokenize
- 3: $w^* \leftarrow [\phi_{TOK}(" . "), \phi_{TOK}([SEP])]$ ▷ Stop Tokens
- 4: $t \leftarrow \text{length}(w) + 1$
- 5: **while** $t < \text{max caption length do}$
- 6: $x_{text} \leftarrow \phi_{EMB}(w)$ ▷ Textual Embedding
- 7: $l \leftarrow \phi_f(x_{vis}, x_{text})$ ▷ Token Logits
- 8: $w_t \leftarrow \eta(l) \in D$ ▷ New token
- 9: $w[t] \leftarrow w_t$
- 10: $t \leftarrow t + 1$
- 11: **if** $w_t \in w^*$ **then break**

In Algorithm 1, an arbitrary sequence P can be introduced to the model to form the starting sequence for captioning. Since token probability prediction is conditional not only on the image features, but also on the preexisting tokens, adding tokens to the starting sequence serves to encourage the model to align its token prediction with this sequence, and to generate relevant textual outputs. We refer to this as *prompting* the textual decoder, and conduct experiments around this capability to explore its application in radiology.

With the captioning formulation in Algorithm 1, we treat *Unprompted* captioning as a special case of prompted captioning where the Prompt P is empty, leaving $w = [\phi_{TOK}([SOS])]$ as our initial prompt token. Only forward captioning is presented, but backward captioning requires

just a change to the w^* special token embeddings, the initialization of w with ". [SEP] ", and $\phi_f \rightarrow \phi_b$. The w^* token embeddings serve to break the prompted captioning process into sentence-length outputs, allowing us to structure a radiology report with multiple prompts, but the ". " can be omitted for full context-length unprompted captioning.

We propose two different methods for prompting. In the first, which we refer to as *Prompted* captioning, we add a word or phrase (typically a pathology of interest) to P , and allow the model to run forward captioning given this starting sequence and generate output tokens w . In the second, which we refer to as *Iterative Prompted* captioning, we follow the *Prompted* procedure, but we prompt the model once more with outputs $w_{i>0}$ in the backward captioning setting. This allows the model to generate additional tokens before and after the initial prompt P . Given the typically rigid linguistics of radiology reports, allowing for forward and backward captioning on the same prompt may allow the generated text to fully describe a finding with similar semantics to those seen during pretraining.

Datasets

We use MS-COCO (Lin et al. 2014) and MIMIC-CXR (Johnson et al. 2019a,b) for pretraining, and transfer our visual encoder to a variety of downstream datasets. Dataset details are described here:

MS-COCO (Lin et al. 2014) comprises natural images each paired with captions. For pretraining the RadTex model, we use the official 2017 split with 118K images.

MIMIC-CXR (Johnson et al. 2019a,b) provides 377,110 chest X-rays (CXRs) with paired reports and CheXpert labels. For pre-training, we use the *Findings* and *Impression* sections and both frontal and lateral MIMIC-CXR-JPG images. Reports are preprocessed to remove references to prior studies in the training and validation sets (train/val/test: 368,960/2991/5159). For downstream classification, we use Pathology9 (Liao et al. 2021), containing 9 of the 14 original CheXpert labels with over 100 test examples.

CheXpert (Irvin et al. 2019) includes 224,316 chest radiographs from Stanford Hospital. Following the official split, our experiments focus on five competition pathologies: Atelectasis, Cardiomegaly, Consolidation, Edema, and Pleural Effusion.

Edema Severity (Hornig et al. 2021) is derived from MIMIC-CXR, grading 7,390 radiographs for pulmonary edema severity on a 0-3 scale (0: none, 1: vascular congestion, 2: interstitial edema, 3: alveolar edema). While most labels derive from regex, the test set ($n = 141$) uses consensus labels from radiologists. This test set is unseen during MIMIC-CXR-JPG pretraining.

RSNA Pneumonia (Shih et al. 2019) comprises approximately 30,000 frontal radiographs from NIH CXR-8 (Wang et al. 2017), labeled for pneumonia presence.

AUC (%)		AUC (%)	
50K	79.3 \pm 0.1	L = 1	79.3 \pm 0.1
100K	80.1 \pm 0.1	L = 2	80.1 \pm 0.1
200K	79.8 \pm 0.1	L = 4	79.7 \pm 0.1

(a) Pretraining Steps

(b) Transformer Layers

AUC (%)		AUC (%)	
SciBERT	79.3 \pm 0.1	Removed	79.3 \pm 0.1
COCO SP	79.4 \pm 0.0	Present	78.7 \pm 0.1
MIMIC SP	79.0 \pm 0.1		

(c) Tokenizer Vocabulary

(d) Prior Report Comparisons

Table 1: Ablation study of RadTex architecture on Pathology9. Average of three trials is reported with Mean \pm SD.

Experiments

We perform an extensive set of experiments to evaluate our model. We run an ablation study on a bicaptioning pretraining architecture to determine the final RadTex model. To assess the efficacy of the vision encoder, we freeze RadTex encoder weights and train a linear classifier, comparing our vision encoder with those from contrastive pretraining on various downstream tasks. Furthermore, we evaluate the interpretability of captioning by prompting the transformer decoder of pretrained RadTex models.

Implementation Details

Images are resized to 224×224 for processing by the vision encoder. The last convolutional layer of the ResNet50 returns spatial image features of size $7 \times 7 \times 2048$.

All models are pretrained with an SGD optimizer with Lookahead ($k = 5$, $\alpha = 0.5$, as in (Zhang et al. 2019)). A linear warmup of the learning rate (5% of total steps) is followed by cosine decay, with maximum LR of 0.4 and 0.002 for visual encoder and transformer decoder, respectively. Models are pretrained on 8 Nvidia V100 GPUs with an effective batch size of 512 samples. We monitor validation loss on the pretraining task and use the best model checkpoint for downstream tasks.

For all downstream tasks, we extract the visual encoder from the pretrained model and freeze model weights. We train a classification head for the visual encoder on a single V100 GPU with a learning rate of 0.02 and batch size of 16, reducing LR by half if validation loss has not decreased after 5 epochs. All reported downstream results are the mean and standard deviation of three trials, unless otherwise stated. We provide our code for reproducibility.

Pretraining Ablations

Prior to the ablation study, we make adjustments to key settings to better suit the general-domain bicaptioning model (i.e. VirTex by Desai and Johnson 2021) for the radiology domain. Specifically:

- Context length: Expanded from 30 to 170 tokens, to encompass 99% of MIMIC-CXR *Findings* and *Impression*.

- **Tokenizer vocabulary:** `scibert_scivocab_uncased` (Beltagy, Lo, and Cohan 2019) used instead of SentencePiece vocabulary (Kudo and Richardson 2018), following Chauhan et al. (2020) for MIMIC-CXR tokenization.
- **Normalization:** Adjusted to match the mean and standard deviation of the MIMIC-CXR-JPG training corpus.
- **Prior reference removal:** Filtered out sentences that reference previous scans using regex.

With these settings as our baseline, we evaluate ablations on Pathology9 classification task as summarized in Table 1.

Pretraining Steps We increase the number of pretraining steps of our baseline model from 50K to 100K and 200K, a change which amounts to an adjustment to the cosine decay scheduler. As shown in Table 1a, we find that both improve downstream classification performance, but the model with 100K steps performs the best.

Transformer Layers Following the ablation study in VirTex (Desai and Johnson 2021), we experiment with additional layers in the transformer decoder. Notably, we observe improvement in the Pathology9 AUC with 2 layers. Results are shown in Table 1b.

Tokenizer Vocabulary We test the new tokenizer against COCO SentencePiece and MIMIC SentencePiece (computed from the MIMIC training corpus). Surprisingly, despite an ability to represent words in radiology reports with fewer tokens given the in-domain vocabulary, the MIMIC SentencePiece model performs worse when it comes to downstream classification (Table 1c). The COCO model performs slightly better than our baseline despite the out-of-domain vocabulary, but by a negligible margin ($p < 0.05$ in a one-sided t-test).

Prior Reference Removal Another key setting for our baseline model is the removal of sentences in the training corpus containing the phrases “prior” and “compar.” We hypothesize that the presence of these phrases trains the model to hallucinate prior studies, of which it could have no knowledge. Removing the phrases is shown to both improve downstream classification (Table 1d) and reduce the number of references to prior reports, but may slightly harm clinical efficacy during captioning (Table 2).

Final RadTex Model Our final RadTex model incorporates baseline settings and findings from the ablation study (100K steps, 2 layers, `scibert_scivocab` vocabulary, priors removed). This model achieves a Pathology9 AUC of 80.5%, which exceeds all other ablations.

For visual encoder quality experiments, we pretrain RadTex on MS-COCO before MIMIC-CXR for better weight initialization. We report these results as RadTex/COCO+MIMIC, or simply RadTex, while the model trained solely on MIMIC-CXR is denoted as RadTex/MIMIC.

Visual Downstream Tasks

To evaluate RadTex’s pretrained visual encoder, we compare to contrastive pretraining, which has previously been shown

Pretraining	Priors (%)	macro-F1
Ground Truth	52.5	—
Unprompted (Priors Present)	43.0	0.254
Unprompted (Priors Removed)	0.1	0.242

Table 2: Removing prior report comparisons reduces hallucinated references. Priors indicate the percentage of reports with prior keywords, and macro-F1 is evaluated against ground truth by CheXpert labeler.

to perform better than captioning pretraining on natural image (Radford et al. 2021) and radiology datasets (Zhang et al. 2022). We compare performance on three downstream classification tasks: CheXpert (multilabel classification on five competition pathologies), RSNA pneumonia detection (binary classification), and Pulmonary Edema Severity classification (multiclass grading).

For a direct comparison of RadTex with contrastive learning, we obtain the final visual encoder weights from CheXzero (ViT-B/32), BiomedCLIP (ViT-B/16), and OpenAI’s CLIP model (ResNet50). CheXzero is initialized from CLIP and pretrained on the Impressions section from MIMIC-CXR; BiomedCLIP, with an initialized text encoder, is pretrained on PMC-15M, with 15 million image-text pairs from PubMed; OpenAI’s CLIP is pretrained on 400M internet-sourced image-text pairs. We use our COCO/MIMIC-pretrained RadTex model for experiments.

To compare RadTex with other models, we freeze visual encoder weights and train a randomly initialized linear classification head on varying amounts of data for each classification task. We use a fully supervised ResNet50 model as a baseline. Frozen linear classification performance is considered to be a good measure of visual encoder performance, as it is a reflection of visual embedding quality.

Figure 3 shows RadTex visual encoder performance against other contrastive methods on downstream tasks. RadTex is competitive, surpassing CheXzero on CheXpert Competition and Edema Severity tasks with most amounts of labeled data, despite CheXzero’s vision transformer architecture and larger size (87.9M vs. 23.5M parameters). RSNA Pneumonia detection yields similar results between CheXzero and RadTex. OpenAI’s CLIP, pretrained on general web data performs poorly on the radiology-domain tasks with a frozen visual encoder.

For RadTex, initialization with pretraining on a natural image dataset does improve performance slightly. In Table 3, we find improvement from RadTex/MIMIC to RadTex/COCO+MIMIC at all labeled data levels. We also compare to a VirTex model, pretrained with the same settings as (Desai and Johnson 2021) on COCO followed by MIMIC-CXR. Improvement from this VirTex/COCO+MIMIC model shows that by optimizing for bi-captioning settings on the *radiology domain*, we achieve better performance.

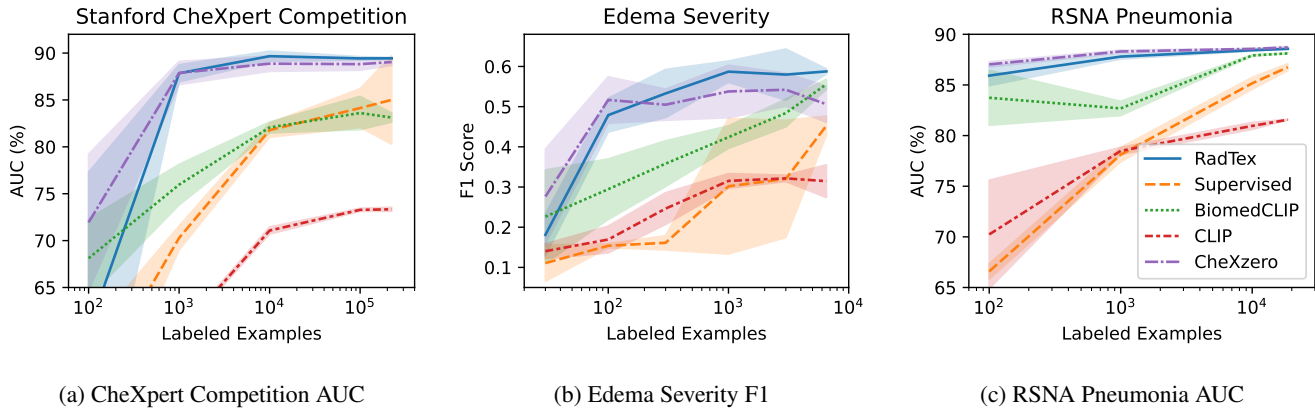


Figure 3: RadTex is competitive with CheXzero and other methods on a variety of downstream classification tasks. RadTex results are for RadTex/COCO+MIMIC pretraining. Downstream tasks are trained in three trials, with Mean \pm SD across 3 runs displayed.

	CheXpert Competition AUC (%)		
	1%	10%	100%
Fully Supervised	71.9 \pm 2.6	82.3 \pm 3.5	85.0 \pm 4.7
OpenAI CLIP	59.8 \pm 0.4	72.4 \pm 0.6	73.3 \pm 0.2
ConVIRT	85.9	86.8	87.3
BiomedCLIP	77.2 \pm 0.9	82.1 \pm 2.6	83.1 \pm 0.5
CheXzero	88.9 \pm 0.6	89.1 \pm 0.2	89.0 \pm 0.4
VirTex	86.6 \pm 0.8	86.7 \pm 0.7	87.3 \pm 0.2
RadTex/MIMIC	88.4 \pm 0.2	89.2 \pm 0.5	89.0 \pm 0.4
RadTex	89.2\pm0.4	89.6\pm0.1	89.4\pm0.1

Table 3: CheXpert linear classification results with variable amounts of downstream training data. Mean \pm SD AUC across 3 trials presented. ConVIRT results are from (Zhang et al. 2022). RadTex (bottom) denotes RadTex/COCO+MIMIC, with VirTex pretrained using identical data.

Interpretable Report Generation

Bicaptioning pretraining enables projection of visual embeddings to interpretable language outputs. Using autoregressive captioning (see Alg. 1), RadTex can produce a radiology report based on visual embedding, with an optional prompt. We explore *Unprompted*, *Prompted*, and *Iterative Prompted* captioning settings. Nucleus sampling, found superior in early tests, is our default sampling strategy over beam search.

When employing Prompted Captioning, any word or sequence of tokens can be used as a prompt, potentially eliciting insights into rare or abnormal pathologies. For optimal clinical efficacy in radiology reports, we use the outputs from a Pathology9 classifier. We determine prompts based on thresholds set by maximizing individual pathology $TPR * (1 - FPR)$ on the validation set, where TPR is the true positive rate and FPR the false positive rate. The model is prompted with only the positive pathologies, and their outputs are concatenated to form the final report.

Measuring Caption Quality We generate captions for 5,159 MIMIC-CXR test set radiographs. Table 4 compares RadTex to some of the best-performing radiology report generation models: M^2 Trans (Cornia et al. 2020; Miura et al. 2021), R2Gen (Chen et al. 2022), and CXR-RePaiR (Endo et al. 2021). Evaluation metrics include BLEU-2 and BERTScore (Zhang et al. 2020) for textual similarity, macro-F1 from the CheXpert labeler, CheXbert similarity, and RadGraph F1 for clinical efficacy. Boag et al. (2020) noted that randomly retrieved reports score surprisingly well on these metrics, and these results are included in our baseline.

RadTex scores well on the five reported metrics across the board. The Unprompted model achieves higher BERTScore and trails only M2 Trans in CheXpert F1 among baseline methods. RadTex Prompted achieves similar RadGraph F1 score to Unprompted, yet Iterative Prompted improves this score, possibly benefiting from its ability to modify textual output with bidirectional captioning.

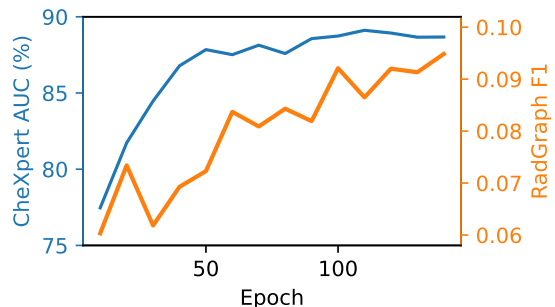


Figure 4: Classification (CheXpert AUC) and Unprompted Captioning (RadGraph F1) performance during RadTex/MIMIC training. Model is trained a total of 100K steps or \sim 140 epochs.

Model	Textual Similarity		Clinical Efficacy		
	BLEU-2	BERTScore [†]	CheXpert macro-F1	CheXbert Sim. [†]	RadGraph F1 [†]
Random Report Retrieval	0.089	0.213	0.177	0.166	0.048
M2 Trans (Miura et al. 2021)	–	0.227	0.304	0.268	0.110
R2Gen (Chen et al. 2022)	0.218	0.186	0.276	0.204	0.057
CXR-RePaiR (Endo et al. 2021)	0.069	0.191	0.256	0.379	0.091
RadTex Unprompted	0.100	0.261	0.289	0.259	0.096
RadTex Prompted	0.069	0.262	0.349	0.336	0.098
RadTex Iterative Prompted	0.082	0.271	0.349	0.333	0.112

Table 4: Comparison of radiology report captioning techniques on a range of metrics. BLEU and BERTScore represent measures of textual similarity, without clinical awareness. CheXpert F1, CheXbert, and RadGraph F1 scores represent measures of clinical efficacy. Other model scores are drawn from existing literature, and we follow their setups as described when comparing RadTex results. [†]Following (Yu et al. 2022a) and using only *Impression* section for ground truth. For BLEU-2 and CheXpert F1 scores, R2Gen and CXR-RePaiR compare to ground truths with both *Findings* and *Impression*, while M2 Trans uses just *Findings*.

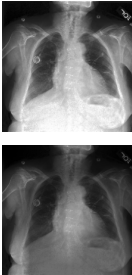
Image and Attention	Ground Truth	Unprompted Report	Prompted Report
	<p>right port catheter tip ends in the mid svc. sternal wires are intact and midline. there are small bilateral pleural effusions, slightly larger on the left than on the right. the cardiac silhouette is moderately enlarged. there is mild engorgement of the pulmonary vasculature. there has been improvement in the previously noted pulmonary edema with minimal residual edema. there is plate-like atelectasis seen in the left base. there is no consolidation or pneumothorax. number. small bilateral pleural effusions. number. improvement in pulmonary edema.</p>	<p>left-sided central venous catheter terminates in the mid svc. overall cardiac size is top normal. aortic knob is noted. patient is status post median sternotomy and intact median sternotomy with intact median sternotomy wires. mediastinal contours are stable in appearance. residual right pleural effusion with airspace opacity seen on the left is present, likely atelectasis. atelectasis is seen at the left lung base. no pneumothorax. if there is a small left pleural effusion.</p>	<p>atelectasis at the left base and no evidence of pneumonia, vascular congestion, or pleural effusion. cardiomegaly is unchanged. pleural effusions have decreased in size and mild cardiomegaly and the previous right lower lobe. pneumothorax in the right lower lobe remain in constant position.</p>

Table 5: RadTex captioning example with CXR image (top) and averaged first layer cross-attention overlaid (bottom) for a sequence of words in the Unprompted Report. Light refers to higher attention.

RadTex Explainability Observations of RadTex reports by authors and an attending radiologist suggest that prompting may improve explainability of the reports. By prompting with a pathology, we aim to probe its visual embeddings and encourage the model to discuss related observations as shown in Table 5. Yet, the radiologist pointed out instances where RadTex generated reports that connected unrelated concepts, such as associating pathologies with no causal link. This underscores the need for better metrics on report explainability, potentially more suited for assistive diagnostics systems than just textual similarity and clinical efficacy metrics.

In Figure 4, we evaluate both linear classification (CheXpert competition AUC) and captioning performance (RadGraph F1) at every 10th epoch during training of RadTex/MIMIC. We find that the capability to differentiate pathologies develops in the model before the ability to mention correct entities and relations in the generated reports. We believe that by re-optimizing RadTex hyperparameters and settings for captioning (including by training the model for longer), we may be able to achieve even stronger captioning performance.

Conclusion and Future Work

In this paper, we show the efficacy of bidirectional captioning as a pretraining strategy for interpretable medical image analysis. Our model, RadTex, not only yields competitive performance against contrastive methods in visual downstream tasks but also surpasses CheXzero on CheXpert and Edema Severity linear classification. A distinct advantage of RadTex is its capability to generate radiology reports, providing levels of interpretability not achieved by other pretraining methods. Additionally, we introduce a flexible prompting mechanism in RadTex for pathologies of interest, demonstrating its potential in improving clinical efficacy.

A future iteration of RadTex could study methods to further improve interpretability. Adopting the strategy proposed by Ramesh, Chi, and Rajpurkar (2022), which involves removing prior references using a token classifier, could further increase temporal consistency and remove hallucinations from report generation. Another promising area of future work is alignment of the visual embeddings with textual encoders for zero-shot classification, or with LLM token embeddings to refine report generation and visual question answering. Recent studies have begun to explore this area, as seen in the work by (Xu et al. 2023).

Acknowledgments

This work was supported in part by MIT Lincoln Laboratory, US Air Force, NIH NIBIB NAC P41EB015902, Wistron, IBM Watson, MIT Deshpande Center, and MIT J-Clinic.

DISTRIBUTION STATEMENT A. Approved for public release. Distribution is unlimited. This material is based upon work supported by the Department of the Air Force under Air Force Contract No. FA8702-15-D-0001. Any opinions, findings, conclusions or recommendations expressed in this material are those of the author(s) and do not necessarily reflect the views of the Department of the Air Force. © 2023 Massachusetts Institute of Technology. Delivered to the U.S. Government with Unlimited Rights, as defined in DFARS Part 252.227-7013 or 7014 (Feb 2014). Notwithstanding any copyright notice, U.S. Government rights in this work are defined by DFARS 252.227-7013 or DFARS 252.227-7014 as detailed above. Use of this work other than as specifically authorized by the U.S. Government may violate any copyrights that exist in this work.

References

- Beltagy, I.; Lo, K.; and Cohan, A. 2019. SciBERT: A Pre-trained Language Model for Scientific Text. In *EMNLP*.
- Boag, W.; Hsu, T.-M. H.; Mcdermott, M.; Berner, G.; Ale-sentzer, E.; and Szolovits, P. 2020. Baselines for Chest X-Ray Report Generation. In *Proceedings of the Machine Learning for Health NeurIPS Workshop*.
- Chauhan, G.; Liao, R.; Wells, W.; Andreas, J.; Wang, X.; Berkowitz, S.; Horng, S.; Szolovits, P.; and Golland, P. 2020. Joint Modeling of Chest Radiographs and Radiology Reports for Pulmonary Edema Assessment. In *MICCAI*.
- Chen, T.; Kornblith, S.; Norouzi, M.; and Hinton, G. 2020. A Simple Framework for Contrastive Learning of Visual Representations. In *Proceedings of the 37th International Conference on Machine Learning*.
- Chen, Z.; Song, Y.; Chang, T.-H.; and Wan, X. 2022. Generating Radiology Reports via Memory-driven Transformer. arXiv:2010.16056.
- Cornia, M.; Stefanini, M.; Baraldi, L.; and Cucchiara, R. 2020. Meshed-Memory Transformer for Image Captioning. arXiv:1912.08226.
- Desai, K.; and Johnson, J. 2021. VirTex: Learning Visual Representations from Textual Annotations. In *CVPR*.
- Dosovitskiy, A.; Beyer, L.; Kolesnikov, A.; Weissenborn, D.; Zhai, X.; Unterthiner, T.; Dehghani, M.; Minderer, M.; Heigold, G.; Gelly, S.; Uszkoreit, J.; and Hounsby, N. 2021. An Image is Worth 16x16 Words: Transformers for Image Recognition at Scale. In *ICLR*.
- Endo, M.; Krishnan, R.; Krishna, V.; Ng, A. Y.; and Rajpurkar, P. 2021. Retrieval-Based Chest X-Ray Report Generation Using a Pre-trained Contrastive Language-Image Model. In *Proceedings of Machine Learning for Health*.
- He, K.; Zhang, X.; Ren, S.; and Sun, J. 2015. Deep Residual Learning for Image Recognition. ArXiv:1512.03385 [cs].
- Holtzman, A.; Buys, J.; Du, L.; Forbes, M.; and Choi, Y. 2020. The Curious Case of Neural Text Degeneration. In *ICLR*.
- Horng, S.; Liao, R.; Wang, X.; Dalal, S.; Golland, P.; and Berkowitz, S. J. 2021. Deep Learning to Quantify Pulmonary Edema in Chest Radiographs. *Radiology: Artificial Intelligence*.
- Irvin, J.; Rajpurkar, P.; Ko, M.; Yu, Y.; Ciurea-Ilcus, S.; Chute, C.; Marklund, H.; Haghighi, B.; Ball, R.; Shpan-skaya, K.; Seekins, J.; Mong, D. A.; Halabi, S. S.; Sandberg, J. K.; Jones, R.; Larson, D. B.; Langlotz, C. P.; Patel, B. N.; Lungren, M. P.; and Ng, A. Y. 2019. CheXpert: A Large Chest Radiograph Dataset with Uncertainty Labels and Expert Comparison. *Proceedings of the AAAI Conference on Artificial Intelligence*.
- Jing, B.; Xie, P.; and Xing, E. 2018. On the Automatic Generation of Medical Imaging Reports. In *Proceedings of the 56th Annual Meeting of the Association for Computational Linguistics*.
- Johnson, A. E. W.; Pollard, T. J.; Berkowitz, S. J.; Greenbaum, N. R.; Lungren, M. P.; Deng, C.-y.; Mark, R. G.; and Horng, S. 2019a. MIMIC-CXR, a de-identified publicly available database of chest radiographs with free-text reports. *Scientific Data*.
- Johnson, A. E. W.; Pollard, T. J.; Greenbaum, N. R.; Lungren, M. P.; ying Deng, C.; Peng, Y.; Lu, Z.; Mark, R. G.; Berkowitz, S. J.; and Horng, S. 2019b. MIMIC-CXR-JPG, a large publicly available database of labeled chest radiographs. arXiv:1901.07042.
- Kudo, T.; and Richardson, J. 2018. SentencePiece: A simple and language independent subword tokenizer and detokenizer for Neural Text Processing. In *EMNLP: System Demonstrations*.
- Li, G.; Duan, N.; Fang, Y.; Gong, M.; and Jiang, D. 2020. Unicoder-VL: A Universal Encoder for Vision and Language by Cross-Modal Pre-Training. *Proceedings of the AAAI Conference on Artificial Intelligence*.
- Li, Y.; Liang, X.; Hu, Z.; and Xing, E. P. 2018. Hybrid Retrieval-Generation Reinforced Agent for Medical Image Report Generation. In *NeurIPS*.
- Liao, R.; Moyer, D.; Cha, M.; Quigley, K.; Berkowitz, S.; Horng, S.; Golland, P.; and Wells, W. M. 2021. Multimodal Representation Learning via Maximization of Local Mutual Information. In *MICCAI*.
- Lin, T.-Y.; Maire, M.; Belongie, S.; Hays, J.; Perona, P.; Ramanan, D.; Dollár, P.; and Zitnick, C. L. 2014. Microsoft COCO: Common Objects in Context. In *ECCV*.
- Lu, J.; Batra, D.; Parikh, D.; and Lee, S. 2019. ViLBERT: Pretraining Task-Agnostic Visiolinguistic Representations for Vision-and-Language Tasks. In *NeurIPS*.
- Mishra, A.; Mittal, R.; Jestin, C.; Tingos, K.; and Rajpurkar, P. 2023. Improving Zero-Shot Detection of Low Prevalence Chest Pathologies using Domain Pre-trained Language Models. arXiv:2306.08000.
- Miura, Y.; Zhang, Y.; Tsai, E.; Langlotz, C.; and Jurafsky, D. 2021. Improving Factual Completeness and Consistency of Image-to-Text Radiology Report Generation. In *Proceedings of the 2021 Conference of the North American Chapter of the Association for Computational Linguistics: Human Language Technologies*.

- Pino, P.; Parra, D.; Besa, C.; and Lagos, C. 2021. Clinically Correct Report Generation from Chest X-Rays Using Templates. In *Machine Learning in Medical Imaging*. Springer International Publishing.
- Radford, A.; Kim, J. W.; Hallacy, C.; Ramesh, A.; Goh, G.; Agarwal, S.; Sastry, G.; Askell, A.; Mishkin, P.; Clark, J.; Krueger, G.; and Sutskever, I. 2021. Learning Transferable Visual Models From Natural Language Supervision. arXiv:2103.00020.
- Ramesh, V.; Chi, N. A.; and Rajpurkar, P. 2022. Improving Radiology Report Generation Systems by Removing Hallucinated References to Non-existent Priors. In *Proceedings of the 2nd Machine Learning for Health symposium*.
- Shih, G.; Wu, C. C.; Halabi, S. S.; Kohli, M. D.; Prevedello, L. M.; Cook, T. S.; Sharma, A.; Amorosa, J. K.; Arteaga, V.; Galperin-Aizenberg, M.; Gill, R. R.; Godoy, M. C.; Hobbs, S.; Jeudy, J.; Laroia, A.; Shah, P. N.; Vummidi, D.; Yadanapudi, K.; and Stein, A. 2019. Augmenting the National Institutes of Health Chest Radiograph Dataset with Expert Annotations of Possible Pneumonia. *Radiology: Artificial Intelligence*.
- Stefanini, M.; Cornia, M.; Baraldi, L.; Cascianelli, S.; Fiameni, G.; and Cucchiara, R. 2023. From Show to Tell: A Survey on Deep Learning-Based Image Captioning. *IEEE Transactions on Pattern Analysis & Machine Intelligence*.
- Tiu, E.; Talius, E.; Patel, P.; Langlotz, C. P.; Ng, A. Y.; and Rajpurkar, P. 2022. Expert-level detection of pathologies from unannotated chest X-ray images via self-supervised learning. *Nature Biomedical Engineering*.
- Vaswani, A.; Shazeer, N.; Parmar, N.; Uszkoreit, J.; Jones, L.; Gomez, A. N.; Kaiser, L.; and Polosukhin, I. 2017. Attention is All you Need. In *NeurIPS*.
- Vinyals, O.; Toshev, A.; Bengio, S.; and Erhan, D. 2015. Show and Tell: A Neural Image Caption Generator. arXiv:1411.4555.
- Wang, X.; Peng, Y.; Lu, L.; Lu, Z.; Bagheri, M.; and Summers, R. M. 2017. ChestX-ray8: Hospital-Scale Chest X-Ray Database and Benchmarks on Weakly-Supervised Classification and Localization of Common Thorax Diseases. In *CVPR*.
- Wang, X.; Peng, Y.; Lu, L.; Lu, Z.; and Summers, R. M. 2018. TieNet: Text-Image Embedding Network for Common Thorax Disease Classification and Reporting in Chest X-rays. In *CVPR*.
- Wang, Z.; Wu, Z.; Agarwal, D.; and Sun, J. 2022. Med-CLIP: Contrastive Learning from Unpaired Medical Images and Text. In *EMNLP*.
- Xu, S.; Yang, L.; Kelly, C.; Sieniek, M.; Kohlberger, T.; Ma, M.; Weng, W.-H.; Kiraly, A.; Kazemzadeh, S.; Melamed, Z.; Park, J.; Strachan, P.; Liu, Y.; Lau, C.; Singh, P.; Chen, C.; Etemadi, M.; Kalidindi, S. R.; Matias, Y.; Chou, K.; Corrado, G. S.; Shetty, S.; Tse, D.; Prabhakara, S.; Golden, D.; Pilgrim, R.; Eswaran, K.; and Sellergren, A. 2023. ELIXR: Towards a general purpose X-ray artificial intelligence system through alignment of large language models and radiology vision encoders. arXiv:2308.01317.
- Yu, F.; Endo, M.; Krishnan, R.; Pan, I.; Tsai, A.; Reis, E. P.; Fonseca, E. K. U. N.; Lee, H. M. H.; Abad, Z. S. H.; Ng, A. Y.; Langlotz, C. P.; Venugopal, V. K.; and Rajpurkar, P. 2022a. Evaluating Progress in Automatic Chest X-Ray Radiology Report Generation. *medRxiv*.
- Yu, J.; Wang, Z.; Vasudevan, V.; Yeung, L.; Seydhosseini, M.; and Wu, Y. 2022b. CoCa: Contrastive Captioners are Image-Text Foundation Models. arXiv:2205.01917.
- Zhang, M.; Lucas, J.; Ba, J.; and Hinton, G. E. 2019. Lookahead Optimizer: k steps forward, 1 step back. In *NeurIPS*.
- Zhang, T.; Kishore, V.; Wu, F.; Weinberger, K. Q.; and Artzi, Y. 2020. BERTScore: Evaluating Text Generation with BERT. In *ICLR*.
- Zhang, Y.; Jiang, H.; Miura, Y.; Manning, C. D.; and Langlotz, C. P. 2022. Contrastive Learning of Medical Visual Representations from Paired Images and Text. arXiv:2010.00747.
- Zhou, L.; Palangi, H.; Zhang, L.; Hu, H.; Corso, J.; and Gao, J. 2020. Unified Vision-Language Pre-Training for Image Captioning and VQA. *Proceedings of the AAAI Conference on Artificial Intelligence*.

Additional Implementation Details

The transformer decoder in RadTex is implemented following VirTex (Desai and Johnson 2021), with a hidden dimension size of 2048, 32 attention heads, and a feedforward size of 8192. Each layer of the transformer decoder includes dropout ($p = 0.1$) subsequent to layer normalization.

VirTex Comparison

When comparing RadTex results to other models on the CheXpert competition classification task in Table 3, we report performance for VirTex. This VirTex model is identical to the architecture presented in Desai and Johnson (2021), but we re-pretrain on MS-COCO, followed by MIMIC-CXR, rather than using VirTex weights. Crucially, we keep the context length at 30 tokens for each of these stages of pretraining. However, because the MIMIC-CXR reports typically span more than 30 tokens, we configure the dataloader to randomly select a sentence from the report when loading a batch. This randomization allows the entire report to be seen during pretraining with many epochs, giving models with shorter context-length a better chance to perform competitively with longer context-length models.

Radiology Report Generation

In this section, we provide additional information on metrics and experiments used to test generated report quality.

Literature Comparisons

In Table 4, we repeat results reported in existing literature. Here, we detail the listed values for R2Gen, M2 Trans, and CXR-RePaiR.

For metrics BERTscore, CheXbert Sim., and RadGraph F1, we take numbers directly from (Yu et al. 2022a) (Supplementary Table 4). These listed scores were based on comparisons to *Impression* section as ground truth, so we only compare to *Impression* when computing our scores using their code. Their scores also represent the average of test set *studies*, rather than images. To select the X-ray used to generate a report for a given study, a PA or AP view image is randomly selected from associated examples. If no PA or AP view is available, a random example from the study is selected. We follow the same selection process when computing these three metrics and comparing to their results.

For metrics BLEU-2 and CheXpert macro-F1, we compute performance on the full number of test set image-report pairs (5,159), and compute BLEU-2 by comparing to the *Findings* and *Impression* sections of the report. We draw numbers for R2Gen from Chen et al. (2022) (Table 2, Base model + relational memory + memory-driven conditional layer normalization), and numbers for CXR-RePaiR from Endo et al. (2021) (Table 1, CXR-RePaiR-2). For M2 Trans, we compute the macro-F1 score based on the per-pathology F1 scores in Miura et al. (2021), Tables 6 and 7 (NLL loss with BERTscore and Entailing Entity Match Reward). BLEU-2 score was not reported for M2 Trans.

Per-Pathology Report Quality

In Table 6, we report the per-pathology breakdown of CheXpert labeling for Unprompted, Prompted, Iterative Prompted, and Random Retrieval captioning methods. For Random Retrieval, we randomly select a report from the training set to use as a baseline for report generation. Beyond CheXpert F1, Precision, and Recall scores, which represent measures of clinical efficacy, we also report the frequency of each pathology in the training dataset. This is computed as the fraction of total 222,750 non-empty ground truth reports that are labeled for a pathology by the Chexpert labeler.

In Figure 5, we plot these results, showing a clear positive trend between the pathology F1 score and training frequency. When pathologies are mentioned more frequently in the training data, they have a higher captioning F1 score in the test data (Unprompted Captioning Pearson $r = 0.92$). This trend holds for all four captioning methods, including Random Retrieval.

Text Generation Examples

Additional examples of radiology report captioning are shown in Table 7, along with decoder attention during *Unprompted Captioning*. We average visual sequence attention across the attention heads from the first layer of the two-layer transformer decoder, and resize the sequence back to the 7x7 visual features output from the ResNet50, normalizing attention between 0 and 1. We can see in the examples that the attention is focused on clinically relevant regions of the chest X-rays: typically over the heart and center of the chest. We find that while attention focuses on relevant portions of the image, it does not move around within the image very much as different tokens are predicted.

When comparing *Iterative Prompted* and *Prompted* captioning results, we observe that iterative prompting does effectively allow for more detailed descriptions of pathologies. By backward captioning with a forward-prompted output, Iterative Prompting yields reports that use modifiers to better describe findings. For example, in Table 7, Iterative Prompting allows for “*interstitial edema...*” (row 1), and “*minimal atelectasis...*” (row 3). We hypothesize that the ability to add modifiers in front of pathology descriptions may contribute to the higher RadGraph F1 score with Iterative Prompting (Table 4).

	Random Retrieval			Unprompted			Prompted			Iterative Prompted			Train Freq.
	P	R	F1	P	R	F1	P	R	F1	P	R	F1	
Atelectasis	0.234	0.271	0.251	0.347	0.423	0.381	0.394	0.729	0.512	0.390	0.749	0.513	0.253
Cardiomegaly	0.276	0.334	0.302	0.369	0.501	0.425	0.440	0.788	0.565	0.430	0.786	0.556	0.292
Consolidation	0.089	0.082	0.086	0.151	0.152	0.152	0.188	0.514	0.275	0.185	0.524	0.274	0.101
Edema	0.265	0.192	0.223	0.468	0.422	0.444	0.475	0.789	0.593	0.472	0.774	0.586	0.287
Enlarged C.	0.088	0.179	0.118	0.086	0.220	0.124	0.099	0.070	0.082	0.087	0.070	0.078	0.095
Fracture	0.019	0.023	0.021	0.085	0.069	0.076	0.031	0.006	0.010	0.023	0.006	0.009	0.026
Lung Lesion	0.042	0.038	0.040	0.086	0.051	0.064	0.057	0.025	0.035	0.074	0.046	0.057	0.036
Lung Opacity	0.324	0.319	0.322	0.398	0.391	0.394	0.450	0.638	0.528	0.443	0.669	0.533	0.255
Pleural Effusion	0.346	0.314	0.329	0.543	0.579	0.560	0.636	0.761	0.693	0.613	0.770	0.683	0.382
Pleural Other	0.057	0.034	0.043	0.049	0.028	0.035	0.079	0.034	0.048	0.055	0.021	0.030	0.013
Pneumonia	0.212	0.175	0.191	0.299	0.236	0.264	0.339	0.633	0.442	0.341	0.583	0.430	0.259
Pneumothorax	0.022	0.041	0.028	0.154	0.275	0.197	0.065	0.901	0.122	0.085	0.632	0.149	0.236
Support Devices	0.284	0.392	0.329	0.523	0.618	0.566	0.675	0.636	0.655	0.663	0.636	0.649	0.308
No Finding	0.186	0.197	0.192	0.396	0.338	0.365	0.562	0.227	0.323	0.535	0.247	0.338	0.334
Macro-Average	0.174	0.185	0.177	0.282	0.307	0.289	0.321	0.482	0.349	0.314	0.465	0.349	—

Table 6: Per-pathology captioning CheXpert label scores for four different methods of captioning on the MIMIC-CXR test set. Training set frequency, as fraction of reports containing Chexpert-labeled pathology, is shown at the right. Enlarged C. stands for Enlarged Cardiome-diastinum. Best F1 Scores for each pathology are **bolded**.

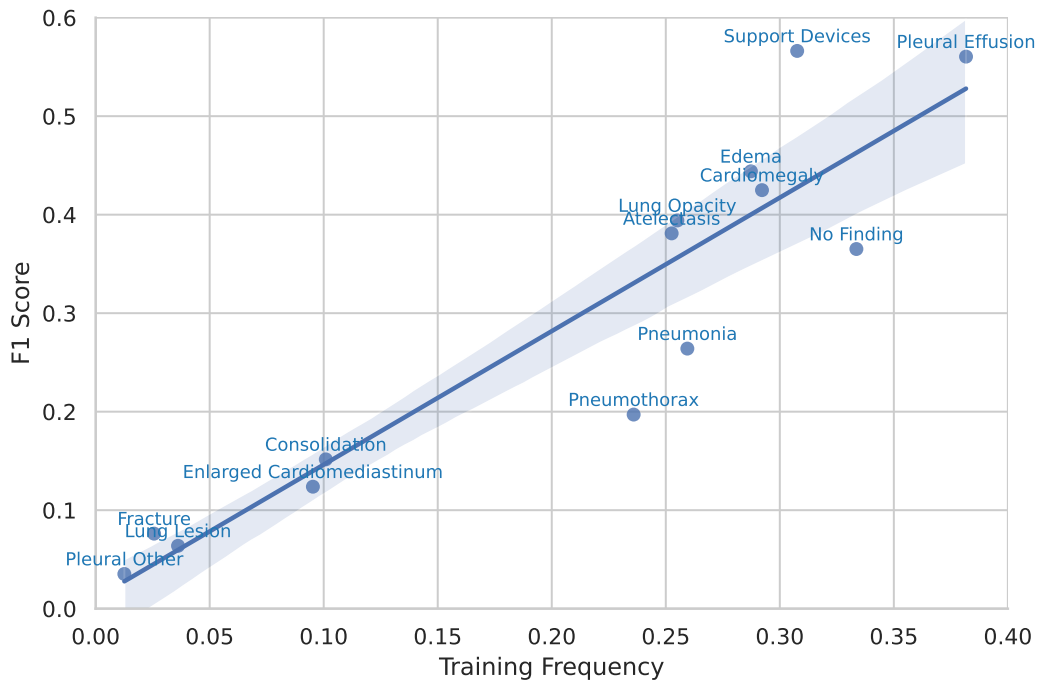


Figure 5: Unprompted Captioning F1 Score vs pathology frequency in training data. Linear regression with 95% confidence interval shown, Pearson $r = 0.92$. Similar trends hold for Prompted ($r = 0.86$), Iterative Prompted ($r = 0.88$), and Random Retrieval ($r = 0.82$)

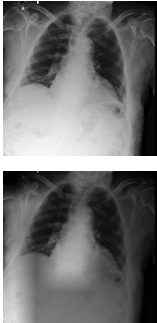
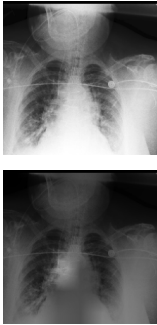
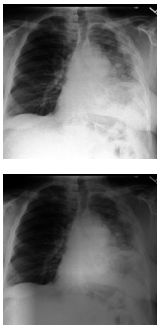
Image and Attention	Ground Truth	Unprompted Report	Prompted Report	Iterative Prompted
	No acute cardiopulmonary process.	there is mild cardiomegaly. the aorta is mildly tortuous . no focal consolidation, pleural effusion, or pneumothorax is seen. the cardiac and mediastinal silhouettes are stable. old healed right rib fractures are present. degenerative changes are seen along the thoracic spine. no acute cardiopulmonary process.	edema is now moderate.	interstitial edema is again seen in the right lung.
	As compared to the previous radiograph, the endotracheal tube, nasogastric tube and right internal jugular vein catheter are unchanged. The pre-existing pulmonary edema might have mildly improved, there is increased retrocardiac and right basal atelectasis. No pleural effusions. No major atelectasis.	mild pulmonary edema has worsened and has not decreased. right lower lobe opacity has probably a combination of pleural effusion or alternatively lymphadenopathy. the catheter has been removed. the heart size is mildly enlarged but is normal. the pulmonary vasculature is not engorged. there is no pneumothorax or pleural effusion. no pneumothorax. sternotomy wires are noted. interval placement of a nasogastric tube whose tip number - up for its tip over number cm. number. et tube ends within number cm above the carina. new right atrium. number.	edema has changed in the patient has worsened since. support devices are unchanged in position.	enteric tube suggests mild pulmonary edema. monitoring and support devices remain in unchanged position, right central venous catheter in place.
	The patient has had a prior left lower lobectomy. Since the prior exam, nodular pleural thickening encasing the left lung has increased at the expense of aeration of the left lung with stable elevation of the left hemidiaphragm. Central adenopathy in the left hilus and adjacent mediastinum has also progressed. The right lung is clear. Cardiomeastinal silhouette is unchanged. Progression of left pleural and nodal metastases.	pa and lateral chest views were provided. there is extensive areas of consolidation in the right lung with a left lung likely representing metastatic lesion . there is a moderate right pleural effusion. there is a large left pleural effusion. there is persistent left effusion. degenerative changes noted in the thoracic spine, better visualized on the right. cardiomeastinal silhouette appears similar. bony structures are intact. the possibility of pneumonia.	atelectasis at the left lung base. consolidation in the left upper lobe is stable. lung opacity is prominent. pleural effusion is volume loss in the right lung. pneumonia or is known between the left upper and has changed in diameter. pneumothorax.	minimal atelectasis at the right lung base. airspace consolidation at the right upper lung is unchanged. left lower lung opacity is concerning for pneumonia, but stable. minimal right basilar loculated pleural effusion and possibly moderate on the left. unchanged right basilar opacity concerning for pneumonia is noted within the left upper lobe. there is no pneumothorax have been stable.

Table 7: RadTex captioning examples with CXR image (top) and overlaid averaged cross-attention from the first layer (bottom), corresponding to a word sequence in the Unprompted Report.